LAWRENCE
LIVERMORE
NATIONAL
LABORATORY

UCRL-JRNL-214285

Preparation Of Polyimide Ablator Coatings Meeting The NIF Specifications

S. Letts, E. Fearon, M. Anthamatten, S. Buckley, C. King, R. Cook

August 3, 2005

Fusion Science And Technology

PREPARATION OF POLYIMIDE ABLATOR COATINGS MEETING THE NIF SPECIFICATIONS

Stephan Letts, Evelyn Fearon, Mitchell Anthamatten,
Steven Buckley, Charlotte King, and Robert Cook

Lawrence Livermore National Laboratory
Livermore, CA 94550

ABSTRACT

We completed the development of a method for preparing smooth vapor deposited polyimide (PI) up to 160 μm thick for NIF target capsules. The process consists of two steps. The first step is vacuum chemical vapor deposition (CVD) of monomer species, pyromelletic dianhydride and oxidianaline, which react on the surface of a shell to form short chain oligomers of polyamic acid. In the second step solvent vapor exposure in a gas levitation apparatus swells and fluidizes the outer surface. Roughness in the outer fluid layer is reduced by surface-tension-driven flow. The shells are cured in the final smoothing step by heating to 300°C reacting the polyamic acid to polyimide. Recent experiments using x-ray radiography have allowed us to determine the depth of solvent penetration and the solvent concentration over a range of solvent exposure conditions. We found that the rate of penetration is a function of the solvent partial pressure in the flowing vapor stream. The concentration of solvent in the swollen layer is 0.45 g/cc and is independent of exposure conditions. Using the penetration information we were able to improve the smoothing process by increasing the solvent partial pressure. The optimized vapor smoothing process allowed us to consistently meet the smoothness specifications of NIF capsules.

INTRODUCTION

Implosion experiments on NIF require capsules to hold the deuterium-tritium fuel and act as an ablator to drive the implosion. The smoothness and uniformity specifications for the capsules are very demanding[1]. Polyimide (PI) is one of the ablator materials under development. Previous investigators demonstrated that it is possible to vapor deposit polyimide onto flat substrates[2, 3]. We and our colleagues at LLE have developed a process to vapor deposit PI up to 160 μm thick onto CH plasma polymer mandrels[4, 5]. The potential benefits of PI are high density (1.43 g/cm^3), the ability to characterize the frozen DT in the shell using optical techniques, the ability to permeation fill, and strength.

During vapor deposition on mandrels we found the coating becomes rough. Using optical microscopy the bumps on the surface were examined and were found to have a visible “root” that leads to an origin that is usually a particle[4, 6]. We found that some surface bumps originate at the inner mandrel surface possibly at dirt particles that are picked up during mandrel handling and storage. Other bumps have an origin in the bulk of the growing film. Our early efforts yielded coatings with many bumps[8]. Gradually our

control over the deposition process and agitation techniques improved resulting in coatings with fewer bumps[7]. We believe the source of the bumps originating within the deposited coating is abrasion or adhesion of growing film to the polymer in the pan holding the shell. Using lower amplitude agitation has been found effective in substantially reducing the number of bumps but not totally eliminating them.

To eliminate the bumps we developed the technique of exposing the coated shell to a solvent vapor to swell the polyamic acid (PAA) coating and allow surface tension to drive the flow of PAA to reduce the surface roughness[6-8]. Previous work in our lab showed that the penetration of dimethyl sulfoxide (DMSO) into vapor deposited PAA follows a frontal mechanism[9]. In frontal diffusion, the rate of solvent penetration is linear with time and the solvent concentration is relatively constant through the swollen layer except for a sudden rise at the "foot" or leading edge[10-12]. Frontal diffusion occurs in polymer-solvent systems in which the diffusion coefficient is a discontinuous function of concentration, initially low and suddenly rising as the solvent front passes. The penetration rate controlling process occurs at the front.

One continuing problem with our smoothing process was poor reproducibility. Characterization was performed on the completed shell only after smoothing and curing. Our goal in this investigation was to better understand the dynamics of the smoothing process by studying the solvent exposed coated shells at intermediate times to determine the concentration and depth of the solvent. Other investigators have used optical methods to characterize the penetration of solvent into polymers[12]. We chose to use a combination of mass increase and radiographic characterization to determine the solvent depth. Radiographic measurements were made possible by the sulfur content of the DMSO, our preferred solvent for vapor smoothing. Using this approach we were able to measure solvent concentration in the swollen polymer and determine the effect of processing conditions on the depth of solvent penetration. The solvent depth was found to correlate with surface smoothness. This enabled us to improve the smoothing process operating conditions and reproducibility.

Solvent Vapor Smoothing

The solvent vapor smoothing process has been found to be very useful in greatly reducing the surface roughness of polyamic acid (PAA) coated mandrels[6, 7]. During smoothing the coated shell is levitated in a flowing gas stream composed of nitrogen and dimethyl sulfoxide vapor. This solvent vapor absorbs into the coating making the outer surface fluid. Surface tension then drives surface fluid flow, which improves smoothness[9]. The absorption of DMSO depends on the shell temperature and the partial pressure of DMSO. The partial pressure of DMSO is determined by the temperature of the reservoir and by the effectiveness of vapor transport to the flowing nitrogen, which is design dependent. One design limitation is that the levitation gas will fully saturate with DMSO only for extremely efficient contact. Our goal was to achieve better smoothing and consistent performance. To better understand the dynamics of smoothing we compared shells smoothed in two different smoothing systems. These design differences will be described next.

Smoother apparatus

We have two different smoothing systems, S1 and S4, with several design differences. S1 was developed more than 3 years ago[8]. The smoother apparatus consists of a reservoir containing DMSO over which a stream of nitrogen flows. The nitrogen flow is controlled with a mass flow controller (MKS 1179A 500 SCCM). The DMSO/N_2 stream then passes through a heated delivery tube and enters the levitator. The levitator is separately temperature controlled. The gas exits the levitator through a nozzle/aperture containing a mesh and a machined hole. The diameter of the hole in relation to the shell diameter is critical to maintaining stable levitation. We use a 2.5 mm hole for our shells, which have a diameter of about 2.3 mm before imidization. Because the gas flow path is short in this smoother design, the nitrogen stream does not become fully saturated. This is a problem we sought to correct in a new smoother design to be discussed next.

The second vapor smoothing system, S4, is shown schematically in Fig. 1. It incorporates several new ideas to achieve more stable levitation, greater temperature stability, and greater vapor contact area to achieve increased solvent saturation. This smoother has a solvent reservoir that is surrounded by a water jacket. Water in the jacket is circulated from a controlled temperature bath. The filtered nitrogen used for levitation ~~also~~ passes through a heat exchange section of tubing approximately 20 cm in length in the water jacket before entering the vapor space above the solvent reservoir at one end. The path length above the reservoir is 10 times longer than S1, allowing the nitrogen sufficient time to equilibrate with the evaporating DMSO solvent. The gas stream next passes into the bottom of the levitation module. The levitator consists of an aluminum cylinder (2 inch diameter by 4 inch length) that is temperature controlled (Cole-Parmer Digi-Sense model 89000-10) using a resistance heater (1/4 by 2 inch 50 watt Omega Engineering) and type K thermocouples for control and temperature sensing. A cross-section view of the levitator is shown in Fig. 2. The gas flow passes through a tapered glass tube (Pasteur pipette, VWR) that fits with close tolerance within the aluminum body of the levitator. The pipette is sealed into the levitator body by wrapping about 3 inches of Teflon tape around the base of the pipette and pressing into the levitator body. A tapering slot in the top of the aluminum body allows illumination and viewing of the levitating shell. The shell is viewed using a long working distance microscope (Navitar) with a CCD camera and video monitor. Rotation of the shell can easily be observed during smoothing and can be controlled by tilting the apparatus. The gas flow rate is adjusted to provide the most stable levitation. Flow is usually set to 380 SCCM during smoothing.

Characterization prior to smoothing

Prior to smoothing we have found it is desirable to limit air exposure to the PAA coated shells. Exposing the shell to humid air results in hydrolysis of the surface and leads to de-wetting during solvent absorption (ref FST 2004). It is desirable to have some information on the mass, dimensions and initial quality of the coating. The shell is characterized on the optical microscope. Focusing at the equator the outer diameter is measured by translating the shell on the encoder stage in the X and Y direction. The shell is then weighed on a microbalance (Cahn 25). From the diameter and mass and knowing the polymer density, we can calculate the thickness of the PAA coating. The entire characterization for surface roughness on the microscope and mass measurement on the

balance takes about 15 minutes. This exposure time has been found to be short enough that de-wetting roughness does not develop during vapor smoothing.

Solvent uptake experiments

A series of experiments were conducted to determine the depth and amount of solvent absorbed during smoothing. Previous experiments have measured roughness as a function of time, and a few experiments were done to measure mass uptake. Using secondary ion mass spectrometry (SIMS) the concentration of DMSO as a function of depth was found to be relatively constant with a sharp drop in concentration at the penetrating front (Lang). However, SIMS is feasible for analysis of initial penetration of up to only 15 μm depth due to limitations in the ability of the technique to etch and analyze materials. We wished to study deeper solvent penetration.

In this experiment we exposed the PAA coated shell in a smoother for a set time period. The shell was then dried on the surface at 80°C for a short time (13 min) to facilitate handling. The shell was next weighed and x-ray radiographed to determine the depth of the solvent penetration. X-ray radiographs were taken using a micro-focus x-ray source (TruFocus, TFX-3065) with a 0.3 mm spot size operating at 15 KeV accelerating voltage and 10 ma current. Exposure time was 7 min. Knowing the mass and depth of solvent allowed us to calculate the concentration of solvent in the swollen layer. The solvent vapor exposures were conducted for several time periods and at several reservoir and levitator operating temperatures. This allowed us to determine the rate of solvent penetration over a range of operating conditions for each smoothing system.

X-ray Radiographic Characterization

Figure 3 shows a radiograph of a PAA layer exposed to DMSO in the smoothing apparatus for 4 hours. The DMSO solvent penetration can be followed because of the sulfur atom present (41 wt% sulfur) in the penetrating molecule. To be more certain we were interpreting the radiograph correctly, we modeled the solvent penetration by calculating the x-ray absorbance for two layers–the outer layer is DMSO-swelled-PAA and the inner layer is PAA. Figure 4 shows schematically the two layers. The cord path length through the shell and the composition of the layers determines the x-ray absorption. X-ray absorption values were taken at the emission wavelength of 8.04 KeV for Cu Kα[13]. Figure 5 shows the calculated x-ray absorption. The peak in absorption occurs at the inner edge of the solvent swollen layer.

All solvent penetration radiographs were analyzed using an optical microscope equipped with a digital camera. The images were computer analyzed (Image Pro-plus). Transmitted light intensity through the radiograph was analyzed by averaging across a short segment. The width was chosen to reduce the grain noise in the image but narrow enough to minimize geometric distortion. Figure 6 shows a typical intensity profile for a solvent smoothed shell. The features of the intensity profile closely resemble the calculated absorption profile. We chose the peak value of the intensity (most absorption) using the image-analyzed graphs. The outer diameter was determined as the point at which the decreasing intensity intercepted the flat background. The inner surface is also easily located as the intensity spike at the inner surface. An intensity spike is also visible at the mandrel-coating interface.

Mass of Solvent

Figure 7 shows the mass of solvent absorbed by a capsule exposed to DMSO vapor. Here we have plotted the solvent mass in the shell as a function of exposure time for several exposure conditions. We found that the absorption of solvent vapor is controlled by the difference in temperature between the reservoir and the shell. Lower temperature difference implies exposure in more saturated conditions.
One of the limiting conditions shown is for shells exposed inside a closed chamber with no gas flow (circles). This represents a limiting case but is not achievable in actual operation because of the need to support the shell in a flowing gas stream. With increased gas flow, boundary layer resistance decreases and absorption rate increases.
All the measurements made on the new, S4, smoother (diamonds) show increasing mass absorption with time and reduced delta T. The old, S1, smoother system is plotted as triangles and shows that this system behaves as if the solvent saturation level is lower than the new smoother.

Solvent Depth and Concentration

Figure 8 shows the solvent depth measured from radiographic images. The general form of the graph resembles the mass data in Fig. 7. Larger delta T reduces the depth of penetration. With both mass and depth information the concentration of the solvent can be calculated. The volume of the layer is calculated using the outer diameter and depth measured from the radiograph. Figure 9 shows the solvent concentration calculated for all tested conditions plotted as a function of temperature difference between the shell and the reservoir. The calculated solvent concentration is essentially constant at approximately 0.45 g/cc. The variations observed are within the experimental error. The limited temperature range used in our smoothing experiments was probably insufficient to test whether the concentration would be temperature dependent.

Capsule Surface Roughness

Figure 10 shows the power spectrum of a series of shells smoothed under conditions using lower saturation, which were then considered our best smoothing operating conditions. Solvent penetration measurements made on shells smoothed using these conditions showed that they were consistent with low solvent partial pressure. By increasing the reservoir temperature we were able to increase the saturation level and increase the solvent mass and depth. We moved from solvent penetration of less than 40 μm to a range of 60 to 100 μm to achieve smoothing that removed middle mode roughness. Shells smoothed using higher solvent partial pressure are shown in Fig. 11. The level of roughness in modes 10 to 60 seen in Fig. 10 has dropped and the shells smoothed in Fig. 11 are now much closer to the NIF standard curve. The smoothness of these shells is 7 nm RMS for modes 12 to 1000.

Summary

Reproducibility of the smoother apparatus was greatly improved by building a new solvent vapor smoothing system that simplified operation and provided greater stability. The new smoother had fewer heat zones and used a water jacket to control the

temperature of the solvent reservoir and eliminate cold spots. The use of the new smoother helped refine the conditions for performing vapor smoothing. Once the smoothing conditions were optimized on the new smoother it provided a platform to conduct smoothing experiments. We measured solvent uptake by mass and radiographic penetration depth measurements. We found that the rate of penetration was a function of the solvent vapor partial pressure, which is determined by the temperature difference between the capsule and the solvent reservoir. The concentration of solvent in the swollen layer was found to be constant over the temperature range studied. Completion of the solvent penetration experiments provided a means of comparing the new (S4) and old (S1) smoother systems. We found that the old system performed in a way that suggested that it had a lower solvent partial pressure. The lower solvent vapor concentration was corrected by raising the reservoir temperature. Ultimately we were able to achieve improved and consistent performance from the old smoother matching the new system. The level of reproducibility and predictability from the two production smoothers improved greatly. Using the improved smoothing operating conditions we were able to reproducibly make shells meeting the NIF specifications.

ACKNOWLEDGEMENTS

This work was performed under the auspices of the U.S. Department of Energy by the University of California Lawrence Livermore National Laboratory under contract W-7405-Eng-48.

REFERENCES

1. S. W. HAAN, T. DITTRICH, G. STROBEL, S. HATCHETT, D. HINKEL, M. MARINAK, D. MUNRO, O. JONES, S. POLLAINE, and L. SUTER, “Update on Ignition Target Fabrication Specifications,” *Fus. Sci. Technol*. **41**, 164 (2002).
2. J. R. SALEM, F. O. SEQUEDA, J. DURAN, W. Y. LEE, and R. M. YANG, “Solventless Polyimide Films by Vapor Deposition,” *J. Vac. Sci. Tech*., **A4**, 369 (1986).
3. V. MALBA, V. LIBERMAN, and A. F. BERNHARDT, “Vapor Deposition Polymerization of Polyimide for Microelectronic Applications,” *J. Vac. Sci. Tech*., **A15**, 844 (1997).
4. C. C. ROBERTS, S. A. LETTS, M. D. SACULLA, E. J. HSIEH, and R. C. COOK, “ Polyimide Films From Vapor Deposition: Toward High Strength, NIF Capsules,” *Fus. Technol*. **35**, 138, (1999).
5. F.-Y. TSAI, D. R. HARDING, S. H. CHEN, T. N. BLANTON, and E. L. ALFONSO, “Effects of Processing Conditions on the Quality and Properties of Vapor-Deposited Polyimide Shells,” *Fus. Sci. Technol*., **41**, 178 (2002).
6. S. A. LETTS, A. H. NISSEN, P. J. ORTHION, S. R. BUCKLEY, E. FEARON, C. CHANCELLOR, C. C. ROBERTS, B. K. PARRISH, and R. C. COOK,

"Vapor-deposited polyimide Ablators for NIF: Effects of Deposition Process Parameters and Solvent Vapor Smoothing on Capsule Surface Finish," *Fus. Sci. Technol*. **41**, 268 (2002).
7. S. A. LETTS, M. ANTHAMATTEN, S. R. BUCKLEY, E. FEARON, A. H. NISSEN, and R. C. COOK, "Progress Toward Meeting NIF Specifications for Vapor Deposited Polyimide Ablator Coatings," *Fus. Sci. Technol*. **45**, 180 (2004).
8. C. C. ROBERTS, P. J. ORTHION, A. E. HASSEL, B. K. PARRISH, S. R. BUCKLEY, E. FEARON, S. A. LETTS, and R. C. COOK, "Development of Polyimide Ablators for NIF: Analysis of Defects on Shells, A Novel Smoothing Technique and Upilex Coatings," *Fus. Technol*., **38**, 94 (2000).
9. M. ANTHAMATTEN, S. A. LETTS, and R. C. COOK, "Controlling Surface Roughness in Vapor-Deposited Poly(amic acid) Films by Solvent-Vapor Exposure," *Langmuir*, **20**(15), 6288 (2004).
10. W. W. MULLINS, *J. Appl. Phys*., **30**, 77 (1959).
11. N. L. THOMAS and A. H. WINDLE, "A Theory of Case II Diffusion," *Polymer*, **23**, 529 (1982).
12. C. J. DURNING, M. M. HASSAN, H. M. TONG, and K. W. LEE, "A Study of Case II Transport by Laser Interferometry," *Macromolecules*, **28**, 4234 (1995).
13. X-ray Cross Section, *CRC Handbook of Chemistry and Physics*, 71st edition, 1990, D. R. Lide ed. P **10**-271.

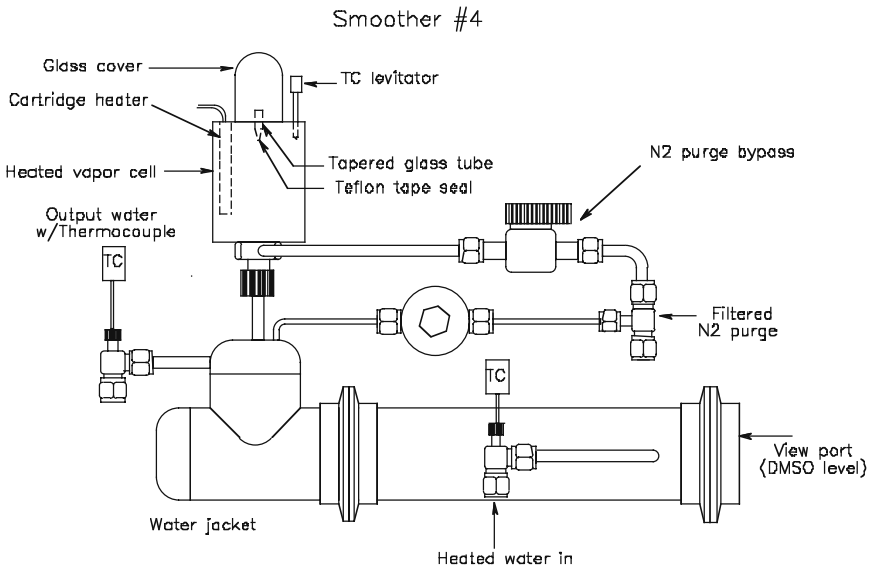

Fig. 1 External view of second smoother, S4.

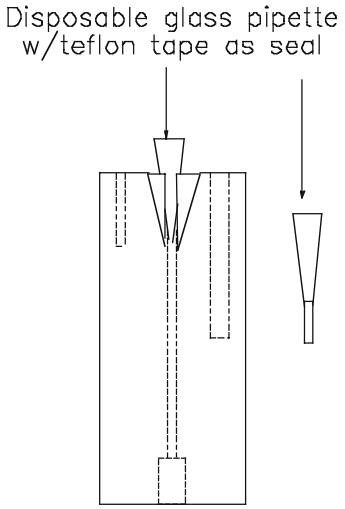

Fig. 2 Cross-section view of levitator portion of smoother S4.

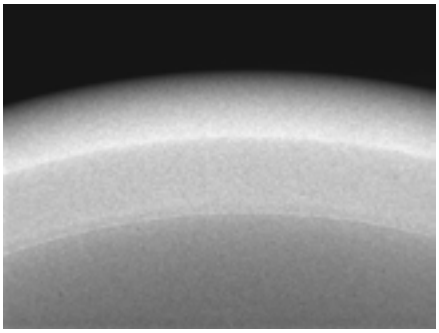

Fig. 3 Radiograph of polyamic acid layer exposed to DMSO is the smoother 4 hrs.

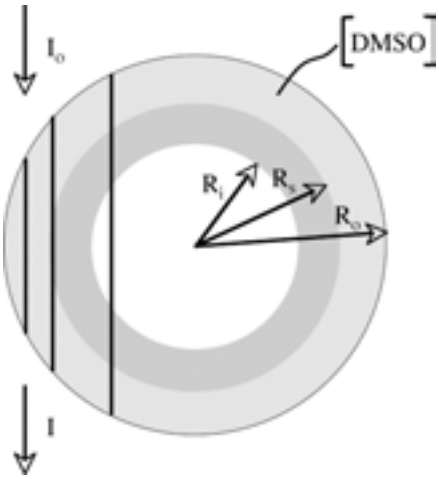

Fig. 4 Schematic representation of two layers used in model of x-ray absorbance. The light gray is DMSO-swelled PAA, dark gray is PAA. The outer, solvent swollen inner and PAA inner radii are marked Ro, Rs, and Ri respectively.

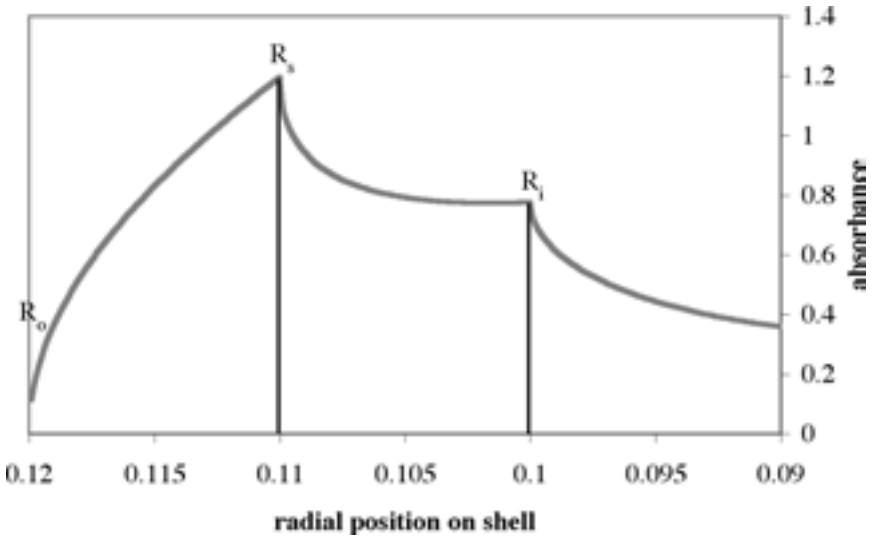

Fig. 5 Plot of calculated x-ray absorption. The peak of absorption occurs at the inner edge of the solvent swollen layer.

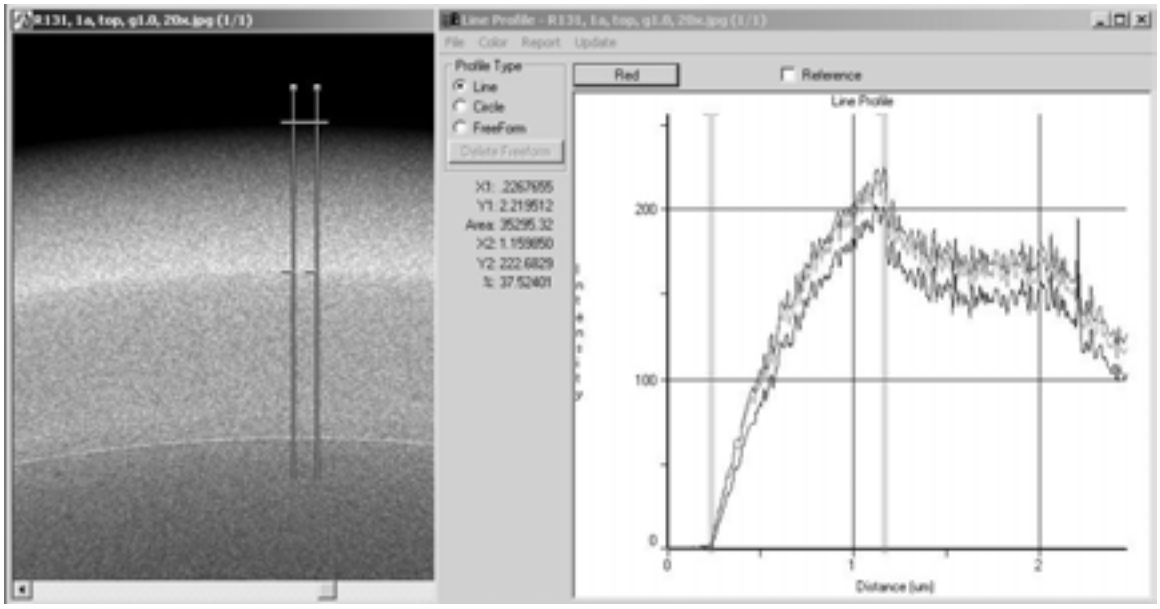

Fig. 6 Typical intensity profile of a radiograph of a solvent exposed shell. The intensity value of the pixels between the vertical bars on the picture are averaged to produce a reduced-noise plot of intensity vs distance on the right. The gray double vertical markers on the plot on the right illustrate selection of the thickness of the solvent swollen layer.

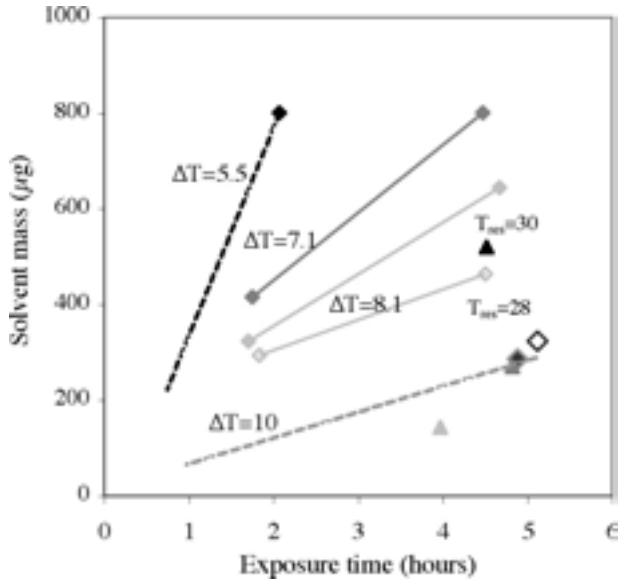

Fig. 7 Mass of DMSO solvent absorbed by a capsule in the smoother. The diamonds plot shells run in the new smoother, S4. The triangles are shells run in smoother S1. ΔT (°C) is the difference between the temperature of the levitator and the temperature of the reservoir.

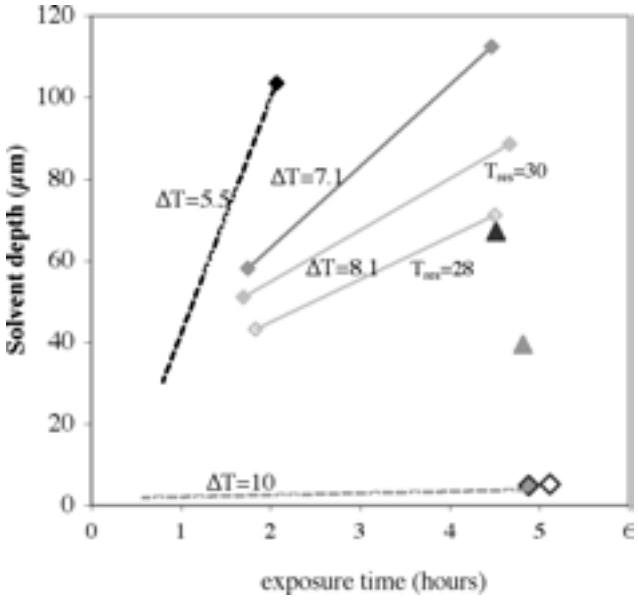

Fig. 8 Solvent depth of DMSO exposed shells in the smoother. The diamonds plot shells run in the new smoother, S4. The triangles are shells run in smoother S1. ΔT (°C) is the difference between the temperature of the levitator and the temperature of the reservoir.

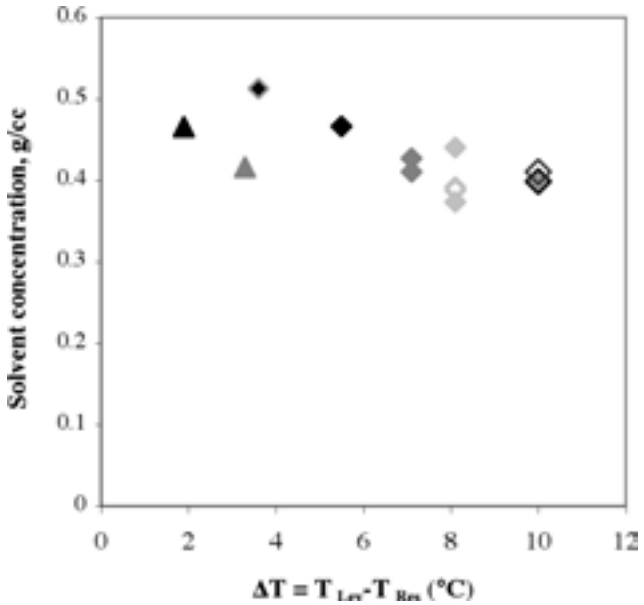

Fig. 9 Calculated solvent concentration for all tested conditions. The diamonds plot shells run in the new smoother, S4. The triangles are shells run in smoother S1. The data represent several different reservoir temperatures.

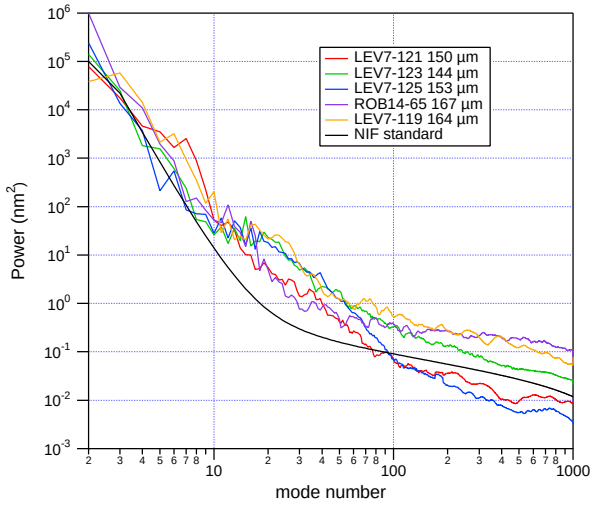

Fig. 10 Power spectra of earlier best-smoothed shells, found to be run under conditions of lower solvent saturation.

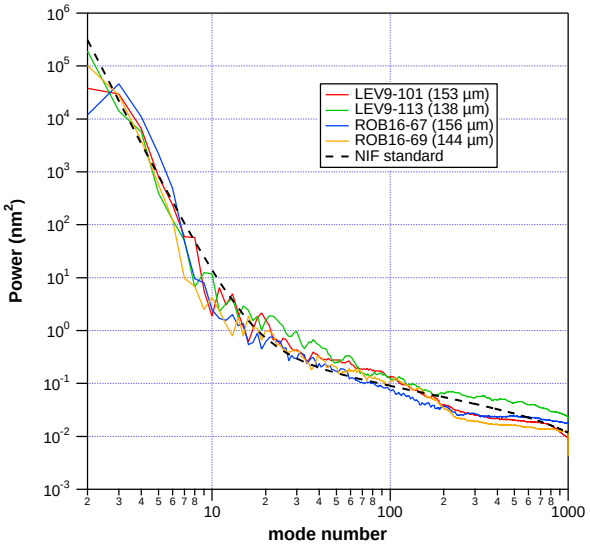

Fig. 11 Power spectra of shells smoothed with higher solvent partial pressure. The middle mode power is much closer to the NIF standard curve.